Available online at www.sciencedirect.com

SCIENCE DIRECT®

Earth and Planetary Science Letters 223 (2004) 79–97

EPSL

www.elsevier.com/locate/epsl

U-series disequilibria in MORB from the Garrett Transform and implications for mantle melting

Frank J. Tepley III[a,*], Craig C. Lundstrom[b], Kenneth W.W. Sims[c], Roger Hékinian[d]

[a] *Earth Sciences Department, University of California, Santa Cruz, 1156 High St., Santa Cruz, CA 95064, USA*
[b] *Department of Geology, University of Illinois, Urbana-Champaign, 245 Natural History Building, 1301 W. Green Street, Urbana, IL 61801-2919, USA*
[c] *Department of Geology and Geophysics, Woods Hole Oceanographic Institution, Woods Hole, MA 02543, USA*
[d] *Keryunan, 29290 Saint Renan, France*

Received 19 June 2003; received in revised form 16 October 2003; accepted 4 April 2004

Abstract

Here, we report $^{238}U-^{230}Th-^{231}Pa-^{226}Ra$ disequilibria and $^{87}Sr/^{86}Sr$ measurements in 11 mid-ocean ridge basalt (MORB) glasses from the Garrett Transform ($\sim 13°30'S$ latitude on the East Pacific Rise [EPR]) whose compositions range from primitive, depleted high-MgO basalts to evolved basalts. U and Th concentrations of samples range between 3 and 75 ppb and between 6 and 220 ppb, respectively, with a corresponding large variation in Th/U (1.5–2.9). $(^{230}Th)/(^{232}Th)$ varies from 1.2 to 1.6 such that $(^{230}Th)/(^{238}U)$ range from $\sim$ 15% excess ^{230}Th in a high-Th/U evolved sample to $\sim$ 25% excess ^{238}U in a high-MgO sample with low Th/U. Out of 11 samples, 7 have ^{238}U excess, an unusual feature for MORB. All samples have ^{226}Ra excesses, with $(^{226}Ra)/(^{230}Th)$ varying between 1.3 and 3.8 constraining ages since eruption to <8000 years and the measured $(^{230}Th)/(^{232}Th)$ to be within a few percent of its value at eruption. $^{87}Sr/^{86}Sr$ ratios range between 0.7022 and 0.7024 and poorly correlate with $(^{230}Th)/(^{238}U)$.

Comparing the Garrett Transform to the Siqueiros Transform shows a remarkable correspondence between sample setting, composition and disequilibria systematics. Both settings produce linear trends of $(^{230}Th)/(^{238}U)$ as a function of Th/U, consistent with mixing between two melts derived from different depths in the melting column. The mixing relationships are identical in both locations: The most incompatible rich samples with the highest Th/U and ^{230}Th excess come from the ridge–transform intersection (RTI), whereas the most incompatible element poor basalts with the lowest $(^{230}Th)/(^{238}U)$ and Th/U are erupted along leaky transform faults. Samples with intermediate Th/U and $(^{230}Th)/(^{238}U)$ all come from within intra-transform spreading centers, consistent with the spreading centers acting to homogenize these diverse magmas. The cause of variation in Th/U could reflect either melting processes or different long-lived sources. No clear indication exists within these data.

Keywords: Garrett Transform; U-series disequilibria; MORB; mantle source heterogeneity

1. Introduction

Mid-ocean ridges are the dominant crust-producing domains on Earth. Adiabatic decompression melting of

* Corresponding author. Tel.: +1-831-459-5228; fax: +1-831-459-3074.
E-mail address: ftepley@es.ucsc.edu (F.J. Tepley).

0012-821X/$ - see front matter © 2004 Elsevier B.V. All rights reserved.
doi:10.1016/j.epsl.2004.04.010

upwelling mantle peridotite produces mid-ocean ridge basalt (MORB). The composition of the melt depends on the source material, degree of melting, depths of initiation and termination of melting, how melt–solid segregation occurs, and extent of fractional crystallization and magma mixing. As numerous studies have demonstrated, considerable chemical and isotopic variability exists in MORB erupted both on and off the ridge axis (e.g., [1–3]). Off-axis basalts (e.g., seamounts and transform basalts) are subject to similar melting processes as on-axis basalts. However, they are less dominated by magma mixing processes [4–6] and thus show an even greater degree of chemical variability [7–14]. However, because only a few of these MORB suites have also been measured for their isotopic compositions of Hf, Nd, Sr, and Pb (e.g., [15]), the extent to which this chemical variability reflects variations in the melting processes, as opposed to variable mixing of melts from depleted (peridotitic) and enriched (pyroxenitic) sources is not well constrained.

There is little debate that compositional variability in some MORB reflects mantle source heterogeneity. Differences in long-lived isotopes occurring over short spatial scales support the proposition of a chemically heterogeneous mantle (e.g., [16–21]). However, the role of melting a heterogeneous mantle in generating uranium series (U-series) disequilibium and trace element fractions in MORB, remains uncertain. Source heterogeneity and its role in melting has been recently addressed by Sims et al. [15] who, based on combined measurements of U-series disequilibria (U–Th–Ra and U–Pa), radiogenic isotopic compositions (Nd, Sr, Hf, and Pb) and major and trace element abundances, propose a mantle source beneath the 9–10°N segment of the East Pacific Rise (EPR) that is chemically homogeneous over the length scale of melting. Furthermore, recent 2D modeling also shows that significant fractionation of trace element ratios and U-series nuclides can occur as a result of melting processes without requiring source heterogeneities [22–24].

U-series disequilibria often are used to constrain the timescales of melt generation, melt ascent processes and differentiation (e.g., [2,3,15,17,20,25–39]). U-series data provide melt generation and ascent constraints because these magmatic processes operate over time scales similar to the half-lives of ^{230}Th ($t_{1/2} \approx 75{,}400$ years), ^{231}Pa ($t_{1/2} \approx 33{,}000$ years), and ^{226}Ra ($t_{1/2} \approx 1{,}600$ years). Thus, studies of disequilibria between daughter and parent isotopes ((^{230}Th)/(^{238}U), (^{231}Pa)/(^{235}U), (^{226}Ra)/(^{230}Th)) can be used to make deductions about magma generation and evolution. Furthermore, because secular equilibrium should exist prior to melting for all the U-series daughter–parent pairs in a mantle source, regardless of enriched or depleted character, observed U-series disequilibria reflect the melting process and not simply source variations.

Although powerful for examining melting processes, U-series disequilibria alone cannot unambiguously distinguish melt generated from a homogeneous source versus that from a heterogeneous source. In particular, variations in Th/U, a ratio of two incompatible elements, could reflect mantle source or could reflect the melting process; discriminating these two alternatives requires complementary measurement of long-lived isotope systems (Sr, Nd, and Pb) indicative of the time-integrated parent–daughter ratios of the mantle sources. When used in concert with U-series isotopes, long-lived isotopic systems enable us to better distinguish between the effects of "source" variability and melting "process" (e.g., [15,17,25,34,40]).

Here, we focus attention on the genesis of melts from a location where magma chamber processes are less active, decreasing the role of magma mixing and accumulation in lessening the magma diversity of the melting column. Specifically, we investigate basalts from the Garrett Transform, which offsets the fast-spreading southern EPR at 13°30′S. We observe correlations between U-series disequilibria, trace element concentrations, and incompatible trace element ratios, which are consistent with mixing between two end-member melts. We also observe distinct ^{87}Sr/^{86}Sr isotopic ratios indicating mantle source heterogeneities. However, the link between U-series disequilibria and source heterogeneity is not clear. These observations closely parallel observations from another intra-transform domain, the Siqueiros Transform (9°N EPR), both in terms of chemical and spatial characteristics.

2. Geological setting and background

The Garrett Transform is located at ~13°30′S on EPR and forms the northern border of the longest, straightest, and fastest portion/segment of the global mid-ocean ridge system (Fig. 1). It offsets the EPR for

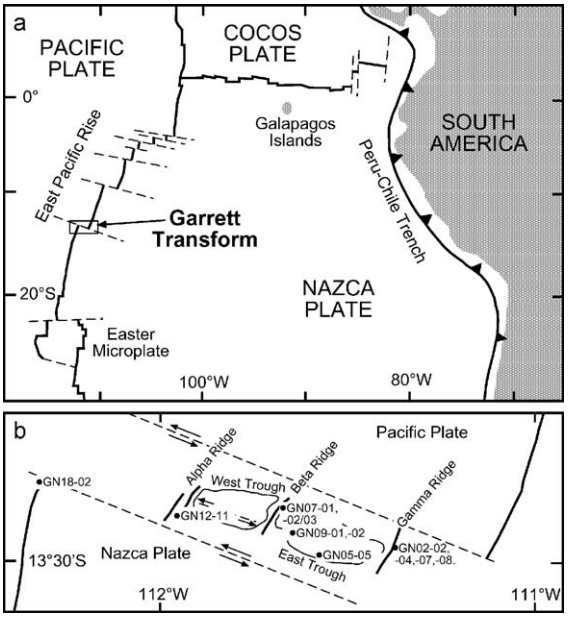

Fig. 1. (a) General location map of the southern EPR and the Garrett Transform. (b) Close-up map of the Garrett Transform showing intra-transform ridges (Alpha, Beta, Gamma) and the transform troughs. General sample locations are illustrated (after [42,44]).

~ 130 km in a right lateral sense and consists of three oblique intra-transform spreading centers (named Alpha, Beta, and Gamma ridges) linked by strike-slip faults and individual transform valleys [41]. Young volcanic rocks (based on submersible observation) occur primarily in intra-transform spreading centers, but are also found as constructional mounds on the floor and along the walls in some of the transform valleys [42–44]. Samples analyzed in this study were collected by submersible in 1991, and their locations are illustrated in Fig. 1b and listed in Table 1. Specifically, we analyzed one sample from the Alpha spreading center, two samples from the Beta spreading center, four samples from the Gamma spreading center, three samples located and presumed erupted along the strike slip fault between Beta and Gamma, and one sample located at the ridge–transform intersection (RTI) with the EPR to the south.

Details of the geology and petrology of the Garrett Transform are described elsewhere [6,42–45]. The lavas of the Garrett intra-transform domain are dominantly olivine and/or plagioclase phyric basalts and picritic basalts [42–44]. They are generally less evolved (Mg# 60–70) compared to adjacent southern EPR samples (with Mg# 50–63 [46]) (Table 2). They have lower concentrations of incompatible trace elements and lower ratios of less/more incompatible elements (K/Ti ratios ~ 0.03–0.1) compared to lavas from the adjacent EPR ridge axis (13 °S to 23 °S; [42–44,46]. The range in major element compositions of the Garrett intra-transform lavas is consistent with crystal fractionation of primary magmas that are not related to the parental magmas of the more evolved lavas erupted at the EPR ridge axis. Additionally, the Garrett lavas are inferred to reflect smaller degrees of melting (< 15%) than typical southern EPR MORB (~ 20%) from a mantle source which has been previously depleted in incompatible minor and trace elements through prior partial melting episodes [42,44,47].

The Garrett Transform is one of the few places where active volcanism occurs along transform faults offsetting major sections of mid-ocean ridge [44]. In this way, the Garrett closely resembles another transform in the Pacific in which systematic sampling and U-series measurements have been made, the Siqueiros

Table 1
Sample locations, rock types and characteristics (from [42,44,45])

GN 02-02	fresh glass, sparsely porphyritic basalt	east flank, Gamma Ridge
GN 02-04	fresh pillow bud, sparsely porphyritic basalt	east flank, Gamma Ridge
GN 02-07	aphyric basalt, fresh sheeted lava	ridge crest, Gamma Ridge
GN 02-08	aphyric basalt, fresh sheeted lava	ridge crest, Gamma Ridge
GN 05-05	porphyritic picrite	southern wall of eastern trough
GN 07-01	lobated flow, sparsely porphyritic basalt	east flank, Beta Ridge
GN 07-02/03	pillow bud, sparsely porphyritic basalt	east flank, Beta Ridge
GN 09-01	basalt	recent lava mound within the eastern trough
GN 09-02	porphyritic picrite	recent lava mound within the eastern trough
GN 12-11	porphyritic basalt	Summit, Alpha Ridge
GN 18-02	aphyric basalt, lobated flow	ridge–transform intersection, near EPR

Table 2
Elemental compositions of glasses used in this study

	GN 02-02	GN 02-04	GN 02-07	GN 02-08	GN 05-05	GN 07-01	GN 07-02/03	GN 09-01	GN 09-02	GN 18-02
SiO_2	50.95	50.58	50.95	50.93	48.67	50.88	51.78	49.73	49.83	50.99
TiO_2	1.21	1.21	1.20	1.20	0.97	1.06	1.10	1.10	1.12	1.87
Al_2O_3	14.62	14.84	14.45	14.78	17.28	15.13	15.15	15.95	16.64	13.65
FeO*	9.30	9.67	9.88	9.53	7.94	8.80	9.39	9.26	8.84	11.90
MnO	0.25	0.17	0.14	0.18	0.16	0.20	0.10	0.19	0.14	0.21
MgO	8.33	8.29	7.97	8.30	9.79	8.65	8.65	8.82	9.02	6.55
CaO	12.41	12.26	12.42	12.20	11.97	12.43	12.74	12.29	12.01	10.62
Na_2O	2.32	2.51	2.40	2.41	2.51	2.30	2.24	2.75	2.85	2.94
K_2O	0.03	0.05	0.04	0.04	0.00	0.04	0.04	0.01	0.03	0.11
P_2O_5	0.09	0.05	0.06	0.06	nd	0.07	0.05	0.05	0.15	0.07
Total	99.58	99.67	99.55	99.66	99.33	99.59	101.28	100.27	100.70	98.95
Mg#	0.64	0.63	0.62	0.63	0.71	0.66	0.65	0.65	0.67	0.52
Ti/U	313	299	312	312	684	393	348		757	150
K/Ti	0.039	0.053	0.05	0.045	0.006	0.05	0.054	0.018	0.037	0.085

No complete analysis of sample GN 12-11 is available (data from [43,45]).

Transform (~ 9°N EPR). These two transforms share remarkable similarity of geological/physical characteristics and chemical compositions of basalts [7,8,10,12,15,20].

3. Methods

We analyzed eleven samples from the Garrett Transform for U–Th–Pa–Ra disequilibria and Sr isotopes by thermal ionization mass spectrometry (TIMS), secondary ion mass spectrometry (SIMS), plasma ionization multi-collector mass spectrometry (PIMMS), and inductively coupled plasma–mass spectrometry (ICP–MS). All of the samples were hand-picked chips of fresh glass (0.3–1.5 g). The details of sample preparation and chemistry followed a modified version of Lundstrom et al. [32], Andrews et al. [48], Pickett et al. [49], Goldstein et al. [27], and Layne and Sims [50]. The details of analytical methods are described in Appendix A.

4. Results

4.1. Concentrations and U-series disequilibria

(^{230}Th)/(^{232}Th) for 7 of 11 samples was measured by SIMS, using the Cameca IMS 1270 at Woods Hole Oceanographic Institution (WHOI) [50] with 2σ errors of 2–5% (Table 3). (^{230}Th)/(^{232}Th) in four samples was measured by PIMMS, using a Thermo-Finnigan Neptune (first at Bremen, later at WHOI) [51] with 2σ errors of 0.3–0.4%. Three samples were measured by both techniques and show good agreement within the analytical uncertainties of the two techniques. Assessing the accuracy of disequilibria measurements in low-concentration MORB requires the use of a rock standard of similarly low concentration, which at present does not exist. Therefore, we have used MORB A2392-9, a glass from the 1991 "Worm Barbeque flow" in the 9°50′N area of the EPR, now measured at several different U-series laboratories (Los Alamos National Laboratory (LANL), WHOI, University of California, Santa Cruz (UCSC)), as our benchmark for determining accuracy of both isotopic and concentration measurements. Our measurement of (^{230}Th)/(^{232}Th) in sample A2392-9 agrees well with previous determinations (Table 3).

Accuracy and reproduction of Th/U is equally as important to precise determination of (^{230}Th)/(^{238}U). Our measured Th and U concentrations and Th/U for A2392-9 show excellent agreement with previous results indicating no bias between the spike calibrations of WHOI, UCSC, LANL, and University of Illinois, Urbana-Champaign (UIUC). Although two separate dissolution Th and U concentration measurements for sample GN18-02 differ by ~ 3%, Th/U reproduces to 1% (2σ). However, reproduction on low-concentration samples is considerably worse. Although U concentrations reproduce to a reasonable

Table 3
U-series and Sr-isotopic results collected from glasses of samples from the Garrett Transform[1]

	Ridge or trough	Th (ppb)	U (ppb)	Th/U	$^{232}Th/^{230}Th_{meas}$	$(^{238}U)/(^{232}Th)$	$(^{230}Th)/(^{232}Th)$	$(^{230}Th)/(^{238}U)$	$(^{234}U)/(^{238}U)$	$(^{226}Ra)/(^{230}Th)$	$(^{231}Pa)/(^{235}U)$	$^{87}Sr/^{86}Sr$[2]
Leaky strike slip												
GN 05-05*	East	18.1	8.7	2.09	130225[b]	1.449	1.429 ± 10	0.986	1.006 ± 62			
GN 09-01	East	6.3[c]	3.1[c]	2.00	116529[b]	1.511	1.597 ± 6	1.057	**1.064 ± 22**			
GN 09-02*	East	14.1	8.9	1.59	125972	1.907	1.475 ± 5	0.773		1.30 ± 13	2.9 ± 1	0.70226 ± 1
					123970[b]		1.502 ± 3		1.011 ± 14			
					127974[b]		1.455 ± 4		0.999 ± 30			
Intra-transform												
GN 12-11	α	68.4	32.9	2.08	123720[b]	1.461	1.503 ± 2	1.029	1.000 ± 11	2.10 ± 2		0.70221 ± 1
GN 07-01	β	36.5	18.3	2.00	131900[a]	1.518	1.410 ± 20	0.929	1.016 ± 30	2.99 ± 2		0.70222 ± 1
GN 07-02/03*	β	37.6	18.9	1.99	127258	1.528	1.461 ± 25	0.956	0.996 ± 13	2.97 ± 2		
					126800[a]		1.466 ± 25					
					133278[b]		1.456 ± 2					
GN 02-02*	γ	48.7	23.2	2.10	136189	1.446	1.366 ± 19	0.945	1.006 ± 12	3.8 ± 3		0.70236 ± 1
					139100[a]		1.337 ± 19					0.70233 ± 1[3]
					133278[b]		1.398 ± 2					
GN 02-04*	γ	52.4	24.3	2.16	133523	1.406	1.392 ± 15	0.991	1.001 ± 20	3.4 ± 2		0.70236 ± 1
					134000[a]		1.387 ± 15					
					133046[b]		1.397 ± 3					
GN 02-07	γ	50.1	23.1	2.17	128500[a]	1.396	1.447 ± 13	1.036		3.46 ± 3		
GN 02-08	γ	49.2	23.1	2.13	136100[a]	1.423	1.366 ± 12	0.960		3.59 ± 2		
RTI												
GN 18-02*	EPR	216.8	75.4	2.88	153150	1.055	1.213 ± 10	1.150	1.004 ± 17	1.5 ± 2		0.70241 ± 1
					151800[a]		1.224 ± 10					
					154500[a]		1.203 ± 9					
2392-9 (9°N EPR)												
This study		118.0	48.2	2.46			1.391			2.71		0.70249 ± 1
Lundstrom et al. [20]		118.9	48.0	2.46			1.391			2.75		
Lundstrom personal communication												0.70251 ± 2
Sims et al. [15]		117.7	47.8	2.46			1.393			2.66		0.70253 ± 3

Th isotopic measurements were made by either [a]SIMS or [b]PIMMS. U and Th concentration measurements by ID-ICP-MS. [c]U and Th concentration measurements by ID-TIMS; [d]$(^{234}U)/(^{238}U)$ measurements made by TIMS. Errors are 2σ variation on last digit(s) given.
East means sample location in Eastern Trough.
Bold font indicates significant sample contamination and therefore not used in figures.

*Concentration reported reflects average of two measurements. Th/U and $(^{238}U)/(^{232}Th)$ errors are estimated at ± 2% in high-concentration samples and ± 4% in low-concentration samples based on external reproducibility. $(^{238}U)/(^{232}Th)$ and $(^{230}Th)/(^{232}Th)$ in the table and in the figures reflect an average of multiple concentration and $^{232}Th/^{230}Th$ measurements where noted.

[1] The following decay constants (/year) were used to calculated activity ratios: $\lambda_{238} = 1.551 \times -10$; $\lambda_{232} = 4.948 \times 10^{-11}$ [109]; $\lambda_{230} = 9.158 \times 10^{-6}$, $\lambda_{234} = 2.8263 \times 10^{-6}$ [110]; and $\lambda_{231} = 2.116 \times 10^{-5}$ [111]; $\lambda_{226} = 4.331 \times 10^{-4}$.

[2] Corrected to NBS 987 = 0.710255.

[3] Wendt et al. [44], corrected to 0.710255.

degree, Th concentrations for GN-05-05 and GN 09-02 differ by ~ 23% and 8%, respectively, indicating the difficulty in achieving excellent sample-spike equilibration for Th and thus concentration reproducibility for these exceptionally low-concentration samples (e.g., [20]). We therefore estimate an error of ± 2% on the Th/U determination for higher concentration samples and ± 4% for lower concentration samples. Although this is a large uncertainty for mass spectrometric analysis, the difference in Th/U in our study is much larger than this uncertainty and does not affect any of our conclusions.

$^{226}Ra/^{228}Ra$ was measured via ion counting TIMS at UIUC. Six samples have counting statistics errors ranging from ~ 0.5% to ~ 1% (2σ) and three samples (GN02-02, GN02-04 and GN18-02) have internal errors ranging from ~ 6% to ~ 10%. Because these latter measurements indicate significant $^{226}Ra-^{230}Th$ disequilibria and therefore constrain the sample age, we have included these data. Our measurement of $(^{226}Ra)/(^{230}Th)$ in A2392-9 agrees within the uncertainties of previous determinations (Table 3). Total error on $(^{226}Ra)/(^{230}Th)$ is ~ 1.5%. Total processing blanks were ~ 150 pg Th and ~ 60 pg U ($n=3$) amounting to < 1% of the Th and U processed for the low-concentration samples and ≪1% for all other samples.

Almost all samples from this study have very low incompatible trace element concentrations and can be classified as depleted MORB (DMORB). The exception is GN 18-02, a differentiated NMORB with 6.5 wt.% MgO and relatively high TiO_2 and K/Ti. All of the DMORB samples are moderately primitive basalts with 8–9 wt.% MgO; GN 09-02 is a basaltic glass having 9 wt.% MgO and large olivines that are likely xenocrystic while GN 05-05 contains embayed xenocrystic olivine [45]. U and Th concentrations discriminate the samples into three groups, which correspond to tectonic setting. Samples interpreted to have erupted along a leaky transform between the Beta and Gamma ridges (GN 09-01, 09-02, and 05-05) all have very low U and Th concentrations (3–9 and 6–20 ppb, respectively). The majority of samples, which come from the Alpha, Beta, and Gamma intra-transform spreading centers, range in concentration from 18 to 33 ppb U and from 36 to 68 ppb Th, while the most differentiated sample, GN 18-02 located at the RTI, has ~ 75 ppb U and 220 ppb Th (Table 3). Correspondingly, Th/U ratios vary between 1.5 in the low-concentration samples to 2.9 in the highest concentration sample. Both the factor of ~ 35 increase in Th concentration and the change in Th/U argue that this variability exceeds that attributable to fractional crystallization.

To assess the role of secondary alteration in our samples, we measured $(^{234}U)/(^{238}U)$. Given the very low concentrations of U and Th in our samples and the relatively high concentrations in seawater and ocean sediments, contamination is indeed a concern. Seawater is enriched in ^{234}U relative to ^{238}U ($(^{234}U)/(^{238}U) = 1.14 \pm 0.03$) [52,53] and any contamination by seawater should manifest itself as elevated $(^{234}U)/(^{238}U)$ in a sample. Measured $(^{234}U)/(^{238}U)$ for all samples but one are within error of secular equilibrium. The one exception to this is the lowest concentration sample GN 09-01 which has a $(^{234}U)/(^{238}U)$ of 1.06, likely indicating contamination of this sample. Therefore, we will not further interpret the disequilibria in this sample, and it is not included in the data presented in the figures. The remaining samples appear to be pristine and therefore good indicators of melt generation and transport. The primary nature of these samples is further reinforced by their trace element systematics and Sr-isotopic compositions.

The disequilibria closely follow the distinction of samples based on concentration and tectonic setting (Fig. 2). Evolved sample GN 18-02, with the highest U and Th concentrations, also has the highest ^{230}Th excess, ~ 15%. The intra-transform spreading centers samples range from slight ^{230}Th excess (~ 4%) to moderate ^{238}U excess (1–7%). Lastly, one sample from the leaky transform has ^{238}U excess of ~ 25% and very low Th and U concentrations.

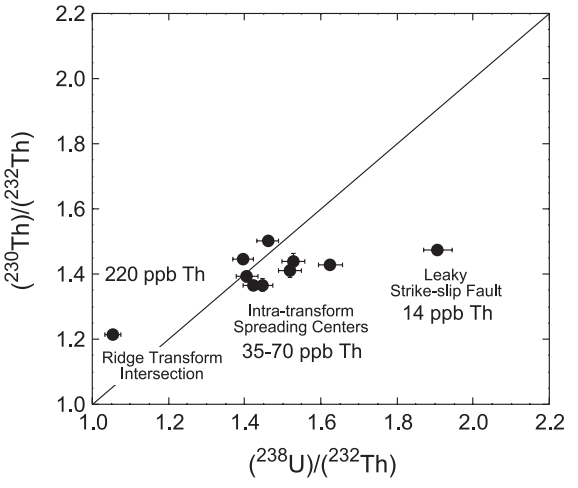

Fig. 2. $(^{238}U)/(^{232}Th)$ versus $(^{230}Th)/(^{232}Th)$ equiline diagram for samples in this study. Parentheses indicate activities. Th concentrations for the different samples illustrates the progression from a depleted end-member to an enriched end-member. Sample GN 09-02 has the lowest Th concentration (14 ppb) and largest ^{238}U excess (~ 25%); $(^{231}Pa)/(^{235}U)$ for this sample is ~ 2.9. Sample GN 18-02, a basalt from the ridge–transform intersection and the most trace-element enriched sample in the rock suite studied, has the highest Th concentration and the largest ^{230}Th excess.

All samples have ^{226}Ra excess, although initial ^{226}Ra excesses in all samples is unconstrained. The presence of ^{226}Ra excess constrains measured (^{230}Th)/(^{238}U) and (^{231}Pa)/(^{235}U) to be close to their eruption values, as ^{226}Ra excess will decay back to secular equilibrium in ~ 8000 years (~ 5× the half-life of ^{226}Ra). (^{226}Ra)/(^{230}Th) range from a low of ~ 1.3–1.5 (GN 18-02 and GN 09-02, the high-Th/U and low-Th/U end-member samples, respectively) to a high of ~ 3.6–3.8 at the Gamma Ridge, values that are among the highest measured in MORB (Fig. 3). There is no correlation between ^{230}Th or ^{238}U excess and ^{226}Ra excess as has been previously noted (e.g., [2,15,20,30]). However, this lack of correlation may be a result of variable sample ages. The lowest Th/U sample (GN 09-02) also has (^{231}Pa)/(^{235}U) = 2.9 ± 0.1. This disequilibrium is higher than (^{231}Pa)/(^{235}U) measurements of 9–10°N EPR (~ 2.7) [15], but similar to the values measured along the Siquieros transform (9°N region [20]).

4.2. Sr-isotope systematics

We measured ^{87}Sr/^{86}Sr via PIMMS (Isoprobe, Field Museum of Chicago) with the details of running conditions in Appendix A. Using a correction offset for our measured NBS 987, sample A2392-9 (9°N EPR) gave a value of 0.70249 ± 2 compared to 0.70253 ± 3 [15]. Additionally, our analysis of GN 02-02 gave a value of 0.70236 ± 1 compared to 0.70233 ± 1 by Wendt et al. [44](Table 3).

^{87}Sr/^{86}Sr varies between 0.70221 ± 1 and 0.70241 ± 1 (Table 3). These values are lower than typical MORB and are consistent with the interpretation of Wendt et al. [44] that magmatism at Garrett Transform reflects melting of a highly depleted source. The variability in ^{87}Sr/^{86}Sr in the Garrett samples, albeit small, exceeds analytical error and therefore indicates that sources with small but differing long-term Rb/Sr contribute to magmas within the Garrett Transform over the scale of a few km to a few tens of kilometers.

The relationship between ^{87}Sr/^{86}Sr and U-series disequilibria is not straightforward (Fig. 4). The most enriched sample (GN 18-02) has the highest Th/U, ^{230}Th excess and ^{87}Sr/^{86}Sr, ~ 0.7024. The lowest ^{87}Sr/^{86}Sr values recorded are ~ 0.7022, and these are for a group samples with modest or large ^{238}U excess (GN 09-02, GN 07-01, GN 12-11). Samples with slight ^{238}U excess or modest ^{230}Th excess have intermediate values of ^{87}Sr/^{86}Sr of ~ 0.7023 (GN 02-02, -04). Overall, there is no correlation (r^2 = 0.16) between ^{87}Sr/^{86}Sr and (^{230}Th)/(^{238}U) indicating that the U–Th

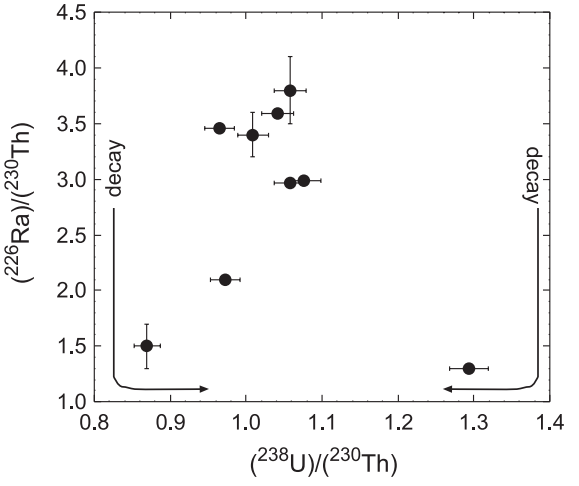

Fig. 3. (^{238}U)/(^{230}Th) versus (^{226}Ra)/(^{230}Th) diagram for samples measured in this study. Arrows indicate the direction to where samples would move during decay. There are no age constraint on these samples, and sample GN 09-02 with high ^{238}U excess but low ^{226}Ra excess may reflect aging.

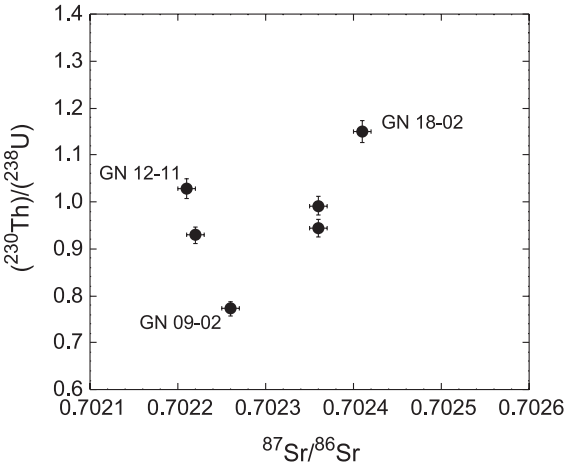

Fig. 4. ^{87}Sr/^{86}Sr versus (^{230}Th)/(^{238}U) for samples measured in this study. Although the correlation is poor (R^2 ~ 0.2), the most enriched sample (GN 18-02) has the highest ^{87}Sr/^{86}Sr, and the most depleted sample (GN 09-02) is among those samples with the lowest ^{87}Sr/^{86}Sr ratio measured in this study.

disequilibria cannot be attributed to simple binary mixing of an enriched and depleted source (Fig. 4).

5. Discussion

5.1. Mixing relationships

Positive correlation between Th/U and (^{230}Th)/(^{238}U) is a ubiquitous observation within MORB studies (e.g., [2,15,17,20,29,30,33,54,55]). Linear correlation on an equiline diagram, where both axes have a common denominator, indicate mixing between chemically distinct melts having differing Th/U and ^{230}Th excess.

The Garrett Transform sample set produces the same trend of higher Th/U having higher (^{230}Th)/(^{238}U). Indeed, the Garrett data show a remarkable systematic correspondence to the data from the Siqueiros Transform in terms of sample geologic setting (Fig. 5). Both the Garrett and Siquieros Transforms produce positive linear correlations of similar slope with samples of the same tectonic setting having identical positions within the trend. For example, samples from the RTI at both locations have the highest Th/U and highest (^{230}Th)/(^{238}U) while samples

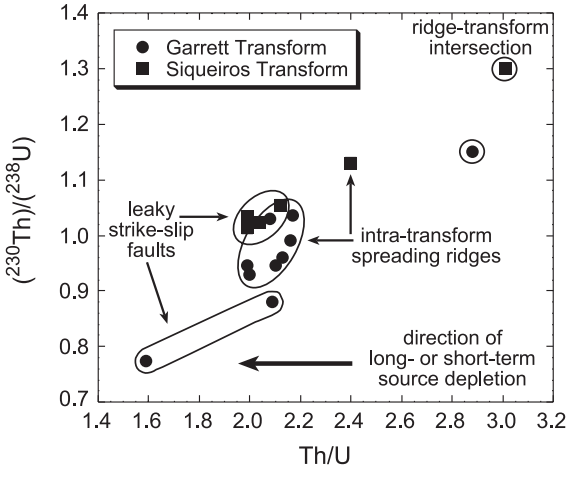

Fig. 5. Th/U versus (^{230}Th)/(^{238}U) for samples from this study and those from the Siqueiros Transform [20]. Good correlation between (^{230}Th)/(^{238}U) disequilibria and Th/U is interpreted to reflect mixing melts produced in different portions of the mantle. Note the geographical similarity of locations in the transform setting of each sample type and their Th/U and (^{230}Th)/(^{238}U).

erupted along the leaky strike-slip faults have the lowest Th/U and lowest (^{230}Th)/(^{238}U). Samples from the intra-transform spreading centers have intermediate values of both Th/U and disequilibria, consistent with being mixes of the RTI and leaky strike-slip fault magmas. The trends of the two transforms differ by the Garrett trend being offset to lower Th/U and (^{230}Th)/(^{238}U), consistent with the greater relative depletion of the Garrett samples (based on incompatible element contents or ^{87}Sr/^{86}Sr).

The chemical and geological correspondence between the Garrett and Siquieros transforms suggests that the dynamics of melting and mixing processes of the two transforms are similar. A general explanation for these parallel trends involves mixing of melts reflecting derivation from different depths in the melting column. Melt containing excess ^{230}Th is often attributed to partial melting in the presence of residual garnet, based upon experimental work showing that $D_{Th}/D_U < 1$ in the presence of garnet [56–59]. Partial melting of garnet lherzolite is capable of generating ^{230}Th excess and is constrained to be ≥ 2.5 GPa ($\sim$ 90 km depth). Melting high-Al, sub-Ca pyroxene at pressures >1.5 GPa has a similar sense of partitioning [60], however, the absolute values of the D's are so low that it would be hard to generate the observed large ^{230}Th excesses by melting of spinel peridotite alone [61]. Based on the "marble-cake mantle" model of Allegre and Turcotte [16], Hirschmann and Stolper [62] suggest that ^{230}Th excess may result from melting of localized garnet pyroxenite veins. These veins are ubiquitous features in mantle peridotite massifs [16], and garnet is stable to shallower depths in mafic than ultramafic sources. Overall, however, ^{230}Th excess is an indicator of melt from greater depth.

^{238}U excess has been measured in relatively few MORB to date [3,63–65]. Explanations for its generation have not been thoroughly discussed (see [3]) but requires $D_{Th}/D_U > 1.0$. Such partitioning fractionation exists for melts in equilibrium with high-Ca, diopsidic clinopyroxene [56,58,59,66,67] such as would be found in spinel peridotite. Indeed, melting of spinel peridotite is capable of creating both ^{238}U and ^{226}Ra excess and transit distances and times could be short to preserve the ^{226}Ra excess.

Alternatively, generating ^{238}U excess may be possible by re-melting previously melted mantle residue. Melting of a depleted source in accordance with dy-

namic melting models (e.g., [68,69]) might yield ^{238}U excess in an instantaneous melt, and this melting model might be valid around a ridge–transform intersection in which the source has already been processed and depleted. However, because such a melting scenario would have problems producing the observed ^{226}Ra excess, we focus this paper on a more general method of producing ^{238}U and ^{226}Ra excesses in MORB.

Thus, these trends can be broadly explained as reflecting mixing between a melt with higher incompatible element concentrations, higher Th/U and greater ^{230}Th excess derived from a greater depth in the melting column and a melt with lower incompatible element concentrations, lower Th/U and lower (^{230}Th)/(^{238}U) derived from a more shallow depth. Since the source for these melts can be assumed to be in secular equilibrium at the initiation of melting, the ^{230}Th–^{238}U disequilibria reflect the melting process, thus providing unique insight into melting.

The interpretation of what the variations in incompatible trace element ratios such as Th/U, Ti/U or K/Ti indicate and the origin of the end-member melts remains hotly debated. The major issue is whether variations in incompatible trace element ratios dominantly indicate variations in source (long-lived source heterogeneity) or simply reflect changes during progressive melting within the melting column. Many studies interpret MORB to represent mixtures of polybaric melts derived from a variably depleted but otherwise homogenous source (e.g., [1,15,70,71]). Trace element diagrams such as Th/U versus Ti/U and (^{230}Th)/(^{238}U) versus K/Ti (Fig. 6) further confirm the binary mixing hypothesis but are ambiguous into whether or not changes in Th/U or other trace element ratios reflects original source variations or melting processes.

U-series studies in the 9–10°N/Siqueiros Transform region of the EPR illustrate both sides of this debate. Limited measurements of Nd and Sr isotopes show significant isotopic variation between the Siqueiros DMORB and EMORB, the Lamont Seamounts and adjacent EPR [8,10,72]. Nevertheless, samples from all of these locations are co-linear on the U–Th isochron diagram [20], interpreted to reflect binary mixing of melts generated by two distinct end-member melting processes that produce differing disequilibria. Because the Siqueiros Transform EMORB with higher $^{87}Sr/^{86}Sr$, Th concentrations and ^{230}Th excesses anchor the high-Th/U end of the trend, these authors suggested that NMORB from the entire 8–10°N EPR area reflected mixing of a melt of ambient peridotite (low-Th/U DMORB end-member) and melt from small-scale long-lived source heterogeneities (high-Th/U EMORB end-member).

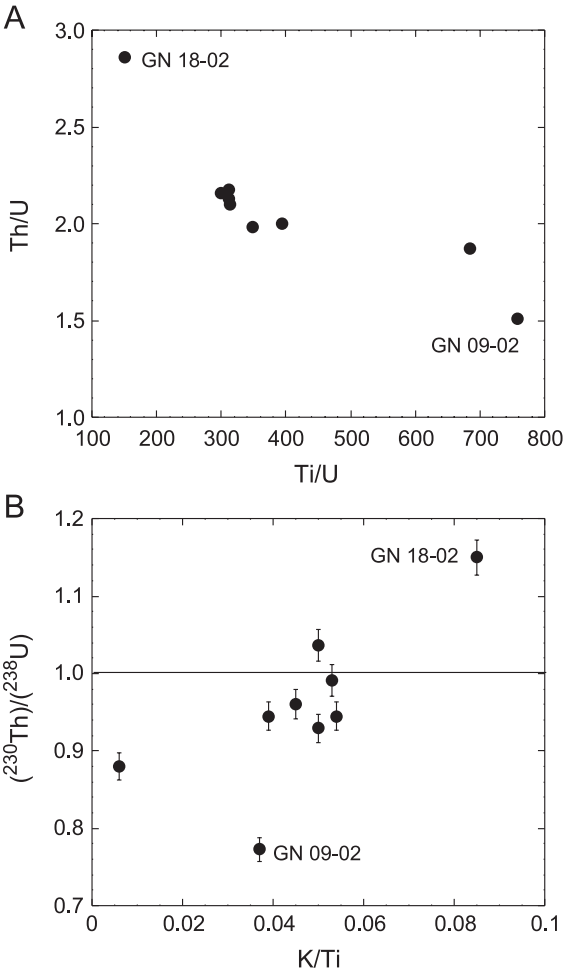

Fig. 6. Correlations of (A) Th/U versus K/Ti and (B) (^{230}Th)/(^{238}U) versus K/Ti illustrate the mixing relationships between melts derived from two separate regions of the melting column or two separate sources. Data from [43,45].

In detail, the Siqueiros DMORB has higher $^{87}Sr/^{86}Sr$ than the EPR NMORB, such that an exact Siqueiros DMORB + EMORB mixture cannot explain NMORB from the 9°N ridge axis (as shown by [15]). However, DMORB from an incipient cone of the Lamont Seamounts (F3-1) has ^{226}Ra excess and low

$^{87}Sr/^{86}Sr$ (Lundstrom, personal communication) like that of the other Lamont lavas (0.7022–0.7025 [8]), making it a possible depleted end-member for the on-axis basalts. By generalizing the model to melting of ambient peridotite (source of low Th/U in DMORB) and mafic veins (source of high Th/U in EMORB), Lundstrom et al. [20] emphasized that the U-series data provided constraint on processes, with all materials beneath the ridge and transform upwelling similarly but with differences in lithology leading to creation of differing disequilibria. Consistent with this model is the observation that data from solely the ridge axis (8°30′N to 10°N) form the same trend as the Siquieros plus Lamont data, with a near-axial EMORB with higher $^{87}Sr/^{86}Sr$ (sample R54-2: 0.7026 analyzed in the Cornell Laboratory [73]) anchoring the high-Th/U end.

More recently, Sims et al. [15] measured a much larger data set of 9–10°N EPR NMORB samples for U-series disequilibria along with Nd, Sr, Hf and high-precision Pb isotopic compositions on the same 9–10°N EPR NMORB samples, as well as several of the Siqueiros DMORB and EMORB samples which had been measured for U-series disequilibria by Lundstrom et al. [20]. Sims et al. [15] showed that Sr, Nd, Pb and Hf isotopic compositions of the 9–10°N EPR NMORB and Siqueiros DMORB samples are essentially homogeneous, but that the Siqueiros EMORB is isotopically enriched. In contrast to the conclusions of Lundstrom et al. [20], Sims et al.'s [15] modeling shows that the U–Th disequilibria and Nd, Sr, Hf and $^{208}Pb/^{206}Pb$ isotopic compositions for the 9–10°N EPR NMORB do not lie on mixing trends between the Siquieros DMORB and EMORB. Based upon this lack of a relationship between these samples' long-lived isotopic compositions and their U–Th–Ra disequilibria, Sims et al. [15] concluded that the melting process such as progressive source depletion during polybaric melting is the dominant control on variations in Th/U. Because the Siquieros EMORB sample is more isotopically enriched, they conclude that the long time-averaged source of this lava has been enriched in incompatible elements, as manifested by its parent daughter ratios Sm/Nd, Rb/Sr, Lu/Hf and Th/U.

Thus, both hypotheses are supported by observation, and distinguishing which interpretation is correct is not straightforward. Mixing of the observed DMORB and EMORB melts from the Siqueiros does not explain the Sr, Nd, Hf and Pb isotope systematics of the 9°N lavas. However, there is reason to believe that there are depleted source components beneath the 9°N ridge axis that produce DMORB having appropriate long-lived isotopic compositions (e.g., Lamont Seamounts). Each interpretation has important implications: if solely melting process can create variations in Th/U and other highly incompatible element ratios, then the interpretation of all trace element variations in MORB need to be reassessed. If on the other hand, variation in Th/U is controlled by long-lived source heterogeneity, then the interpretation of Lundstrom et al. [20] that only 5% of the volume of MORB (the EMORB component) contributes more than 50% of the incompatible element budget requires fundamental reassessment of conclusions about the melting depth (i.e., garnet signature) of the majority of solid beneath a mid-ocean ridge.

If source heterogeneity is present and influencing the generation of U-series disequilibria, what are the possible explanations for the observed de-coupling between U-series disequilibria and long-lived isotope tracers? In a global context, $^{87}Sr/^{86}Sr$ vary systematically with Th/U for MORB, OIB and Pacific plate seamounts producing a hyperbolic curve (Fig. 7). The

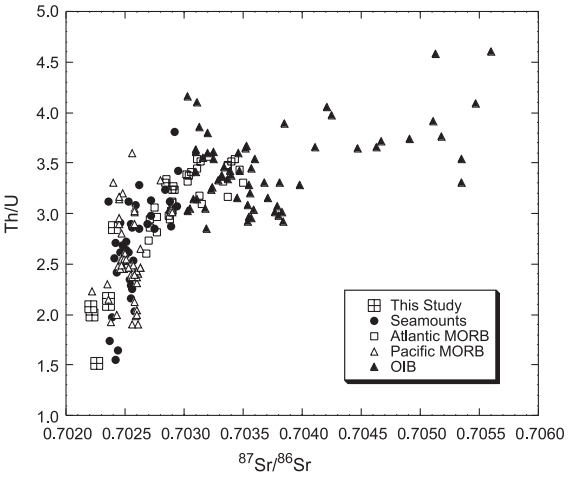

Fig. 7. Global correlation of Th/U versus $^{87}Sr/^{86}Sr$ for basalts derived from the oceanic mantle. Data from [2,8,17,19,20,25,27,28,33,36,55,63,95–108], Lundstrom (unpublished), Hanan (unpublished) and Perfit (personal communication, 1997). Note the strong curvature within the data consistent with observed range in variation of Sr, U and Th in the mantle. If these data reflect mixing of melts, the range in Th/U implies significant variation in Th/U in the source supplying the depleted melt to MORB.

curvature can be matched using a mixing model where the end-member melts correspond to the concentrations of the most depleted and enriched basalts found in Pacific seamounts [74]. In this context, the Garrett Transform samples fall near the depleted low-Th/U end of the curve but show variation in $^{87}Sr/^{86}Sr$, similar to Pacific MORB as a whole or Pacific seamount data as a whole. If the low-Th/U end-member does represent melting of ambient peridotite, then this peridotite end-member must itself be quite variable in $^{87}Sr/^{86}Sr$. If so, discerning coherent mixing relationships between U-series disequilibria and long-lived isotopes will require much larger data sets for a given area of ridge (similar to the Sims et al. [15] data set), which draw from all types of samples from that location (i.e., on and off axis MORB, seamounts and transforms).

A second possibility to be tested is that there is an inherent difference between how $^{87}Sr/^{86}Sr$ records mixing and melting of heterogeneous sources compared with other isotopic tracers such as Nd. Sr is more diffusively mobile than Nd, and may be influenced by the diffusive infiltration of alkali (DIA) process, hypothesized to occur in the shallow ridge melting column [74]. Measurements of Sr diffusion coefficients in alkalic basalt–tholeiitic basalt diffusion couples show Sr to diffuse faster than most cations in silicate melts and similar to the fastest diffusing elements, the alkalis [75]. Thus, it is possible that the variation in $^{87}Sr/^{86}Sr$ observed in the low-Th/U end-member in Fig. 7 reflects the effects of the DIA process in influencing the $^{87}Sr/^{86}Sr$ of the ambient peridotite end-member. If so, then assessment of the mixing behavior of ε_{Nd} with Th/U should produce a tighter array in terms of variation in ε_{Nd}. Unfortunately, there are far fewer combined $(^{230}Th)/(^{238}U)$–ε_{Nd} data sets than there are $(^{230}Th)/(^{238}U)$–$^{87}Sr/^{86}Sr$ data sets.

The conclusion about the role of source heterogeneity in influencing U-series systematics in the Garrett Transform and globally remains ambiguous. Both source heterogeneity and melting process are likely to influence the MORB systematics to differing degrees in different settings. However, the data presented here continue to reinforce the major conclusion of a systematic relationship between $(^{230}Th)/(^{238}U)$ and Th/U reflecting mixing between two melts derived from different depths in the melting column. Indeed, the Garrett data more strongly indicate the difference in melting depths of the end-members. The high-Th/U end-member reflects melting at greater depths because its ^{230}Th excess reflects melting in the presence of garnet ± aluminous clinopyroxene [56–59,61]. Most importantly, in the Garrett case, the low-Th/U end-member has significant ^{238}U excess and therefore cannot result from any melting at garnet-stable pressures; instead, it must reflect melting at depths more shallow than ~ 60 km where garnet or fertile aluminous clinopyroxene is no longer present (e.g., [60]).

5.2. Source/melting relationships

The extent of U-series disequilibria in the Garrett Transform is dependent on the mantle source region, mantle upwelling rate, melting column length, and the depth of initiation of melting. All samples in this study have ^{226}Ra excesses and one sample has ^{231}Pa excess, placing additional constraints on parameters of melting. Additionally, the U-series disequilibria are in part governed by the melt generation and transport mechanism. Traditional melting models (batch or fractional) rely on net retention of one nuclide in the mantle residue after melting to produce fractionation and therefore disequilibria. Bourdon et al. [3] demonstrated that 20–30% ^{230}Th excess, amounts commonly observed in MORB, can be generated through 10% batch melting of a garnet pyroxenite. However, large ^{231}Pa and ^{226}Ra excesses are difficult to explain by simple batch melting [15,34,37,40]. Rather, observed disequilibria are best explained by ingrowth melting models (e.g., [68,69,76,77]), which reflect mass conservation during the dynamic process of melt moving relative to solid.

Two end-member ‘‘equilibrium partitioning’’ ingrowth melting models exist. In one, melt migrates to the surface chemically isolated from the solid matrix after segregation (dynamic melting; e.g., [68,69,76]). In the second, melt continuously re-equilibrates with the matrix as it moves through the melt column (equilibrium percolation models; e.g., [77]). The dynamic model creates ^{226}Ra–^{230}Th disequilibria at the bottom of the melting column and therefore requires extremely high rates of melt transport to preserve the ^{226}Ra excess at the surface. Alternatively, the equilibrium percolation model accounts for ^{226}Ra–^{230}Th disequilibria by creating both ^{226}Ra and ^{230}Th excesses throughout the melting column, even near the top, so that fast melt transport velocities are not required [77].

We are primarily interested in whether melting models are capable of reproducing the observed ^{238}U, ^{231}Pa and ^{226}Ra excesses similar to the DMORB lavas of the Garrett Transform. Melts with these disequilibria are predicted to be in equilibrium with high-Ca, diopsidic clinopyroxene in which $D_U < D_{Th}$ [56,58,59,66,67] like depleted spinel peridotite. We ignore modeling of any ^{230}Th excess, as this is minor at Garrett and attributed to melting in the presence of garnet. For simplicity, we assume a long-term homogeneous mantle source (i.e., constant Th/U) and fixed bulk partition coefficients for each nuclide in both depleted spinel peridotite and residual harzburgite mantle (both D's dominated by modal clinopyroxene) and use single stage melting calculations with a fixed rate of melt productivity. Note that while recent MELTS calculations predict significant variations in the melt productivity as a function of depth [78], for simplicity, we use a fixed rate of melt productivity. We set the bulk U, Th, Ra and Pa partition coefficients at 0.001, 0.002, 0.00001 and 0.00001, respectively. Although the bulk partition coefficients for Ra and Pa are poorly constrained, the uncertainty in D_{Ra} and D_{Pa} has little effect, as long as these elements are an order of magnitude less compatible than their parents, Th and U. We constrain the depth of melting to be within the spinel lherzolite field, and therefore test the melting models between two extreme end-member depths: (1) at ~ 25 kb (~ 85 km melting column), the bottom of the spinel lherzolite stability field; and (2) at ~ 6 kb (~ 20 km melting column), the top of the spinel stability field. The maximum degree of melting for all calculations is based on a prescribed melt productivity of 0.4%/km [1]. Target disequilibria data are $(^{230}Th)/(^{238}U) = 0.75$, $(^{226}Ra)/(^{230}Th) = 3.0–3.5$ and $(^{231}Pa)/(^{235}U) = 2.8$.

First, we tested the dynamic melting model using the analytic solution presented by Richardson and McKenzie (Eq. (17) in [79]) based on the model of McKenzie [76]. We used the criteria discussed above and bracketed the test with reasonable porosities (0.1–10%), upwelling velocities (0.1–10 cm/year) and melt productivity (0.4%/km [1]). Results show that the target ^{230}Th–^{238}U disequilibria can be generated along both a ~ 85 km melting column ($F = 0.34$) and a ~ 20 km melt column ($F = 0.08$) at reasonable porosities (0.1–0.2%) but at extremely small upwelling velocity (0.1–0.2 cm/year). Additionally, it is difficult to match target ^{226}Ra–^{230}Th disequilibria at reasonable upwelling velocities and porosities, and virtually impossible to match target ^{231}Pa–^{235}U disequilibria.

Melting column length makes no difference in dynamic melting models; the disequilibria produced between different column lengths are the same because in these models, the disequilibria are only created at the initiation of melting. Once the parents and daughters are in the melt, and this happens quickly in this "near fractional" situation, the elements' residence time difference cannot be changed. Because of the inability of the dynamic melting model to reproduce target ^{238}U excesses at reasonable upwelling velocities or target ^{226}Ra and ^{231}Pa excesses, we investigated a different model of melt transport.

Alternatively, we explore the equilibrium percolation melt transport model of Spiegelman and Elliott [77] using UserCalc 2.0 [80]. Fig. 8 presents results of the calculations using melting columns of 20 and 85 km in length presented as a function of the solid upwelling velocity (cm/year) and maximum porosity. First-order observations are (1) target ^{238}U excesses may be produced in both melting columns at reasonable porosities (0.1–0.2%) and upwelling rates (0.1–2.0 cm/year); (2) target ^{226}Ra excesses may be produced in both melting columns at low porosities ($\leq 0.1\%$) and variable upwelling velocities (0.1–10.0 cm/year); and (3) target ^{231}Pa excesses are difficult to produce except at low porosities ($< 0.1\%$).

Target disequilibria activity contours change only slightly between the different melting column lengths. This suggests that the entire spinel lherzolite stability field may equally create ^{238}U, ^{226}Ra and ^{231}Pa excesses similar to those observed. Secondly, the $(^{230}Th)/(^{238}U)$ activity contours behave in two different manners: One in which the activity depends on porosity (region of upwelling velocity of 0.1–1.0 cm/year) and one in which the activity depends on upwelling rate (1.0–10 cm/year) (Fig. 8). $(^{226}Ra)/(^{230}Th)$ and $(^{231}Pa)/(^{235}U)$ activity contours change only slightly between melting column lengths and mostly depend on porosity alone.

The end-member criteria ($(^{230}Th)/(^{238}U) = 0.75$, $(^{226}Ra)/(^{230}Th) = 3.0–3.5$ and $(^{231}Pa)/(^{235}U) = 2.8$) define a rather small range of upwelling velocities and maximum porosities. Upwelling velocity ranges from ~ 1 to 2 cm/year, and maximum porosity from < 0.1 to 0.2%. The southern EPR full spreading rate, away from the Garrett Transform, is ~ 15 cm/year, which is

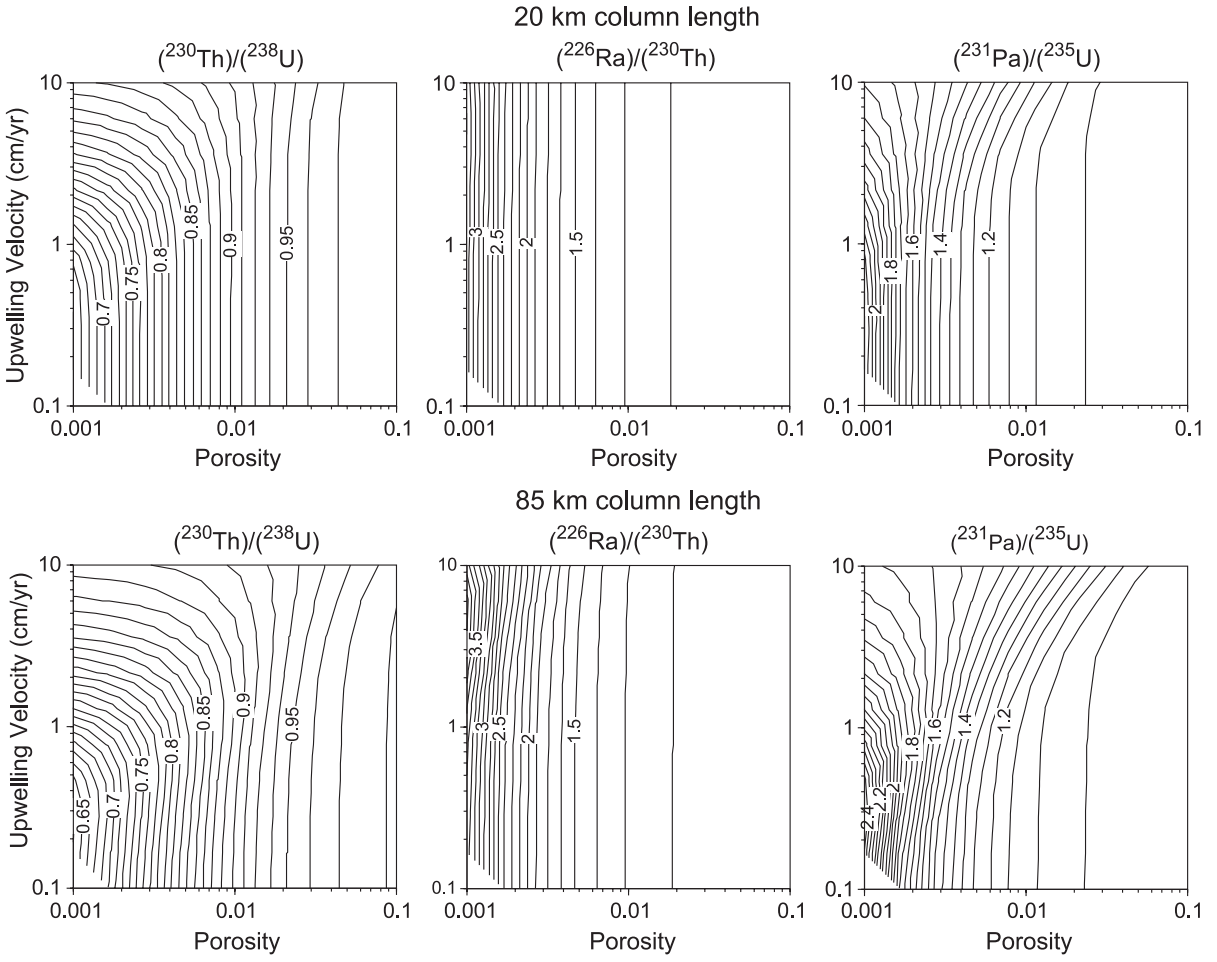

Fig. 8. Modeling results from UserCalc 2.0 from Spiegelman [80]. Contours of activity ratios for (^{230}Th)/(^{238}U), (^{226}Ra)/(^{230}Th) and (^{231}Pa)/(^{235}U) for melts initiated at 25 kb (~ 85 km melt column) and 6 kb (~ 20 km melt column) hypothetically bracketing the spinel lherzolite stability field in the mantle. A parameter space of porosity and upwelling velocity provides possible solution to the observed disequilibria.

~ 15 × faster than the upwelling rates obtained from the modeling. Nonetheless, it is a measure of the robustness of the model that the target ^{238}U excesses may be produced in each melting column. Since the upwelling rate parameter effectively controls the melting rate in our model (because productivity is held constant), another way of interpreting this result is that the productivity could be lower than the assumed (0.4%/km) and upwelling rate correspondingly higher.

We conclude that the samples with ^{230}Th excess are consistent with inclusion of some melt generation in a source region with D_U/D_{Th}>1.0 such as enriched garnet-bearing pyroxenite veins or garnet-bearing lherzolite regions of the deep mantle. Based on equilibrium percolation modeling, we also conclude that samples with ^{238}U excess and accompanying large ^{231}Pa and ^{226}Ra excesses are consistent with melt being derived exclusively from shallow spinel lherzolite.

5.3. U excess and arc lavas

Most MORB lie to the left of the equiline in the ^{230}Th excess field ((^{230}Th)/(^{238}U)>1). However, there are a few MORB samples with recorded ^{238}U excesses ((^{230}Th)/(^{238}U) < 1). Examples include one sample from the FAMOUS zone of the Mid Atlantic Ridge

(MAR; 36°50′N [63]), one sample from the MAR at 29–30°N [3], four samples from the Kolbeinsey Ridge 67–70°N, north of Iceland [64] and a few samples 15–30 km off the 9°30′N portion of the EPR [65]. These ^{238}U excesses range from 2% to ~11% (one at 15% [65]). Several of our samples have similar ^{238}U excesses. Remarkable among our samples is one with ~25% ^{238}U excess, the largest ^{238}U excess and lowest U concentration in MORB reported in the literature to our knowledge.

Our observation of depleted basalt having large ^{238}U excess bears on the interpretation of ubiquitous ^{238}U excess in arc basalts, and on the inferred time scales of fluid transfer, melting and melt ascent. In the arc environment, low-Th/U samples often have up to 60% ^{238}U excess. U has been shown to be highly mobile in hydrous fluids [81,82], and the typical explanation for ^{238}U excess in arcs is preferential mobilization of U by dehydrating fluids from a subducting slab to the magma generation zone in the overlying mantle wedge (e.g., [83–94]). Discerning whether ^{238}U excess reflects recent fluid addition wholly is a critical piece of information in constraining the time scales of addition of materials contributed from the subducting slab. We have demonstrated that mantle melting of dry depleted peridotite has the ability to produce large ^{238}U excess.

6. Conclusions

1. The observed correlations between U-series disequilibria, trace element concentrations and incompatible trace element ratios in Garrett Transform lavas suggest generation of two end-member melts: one with ^{230}Th excess, high Th and U concentrations and high K/Ti, and another with ^{238}U excess, low Th and U concentrations and low K/Ti. These observations closely parallel observations from the Siqueiros Transform in terms of their relationship between chemical characteristics and geological setting.
2. ^{230}Th excesses are consistent with some of the melt generation occurring in a source region with $D_U/D_{Th}>1.0$ such as garnet lherzolite mantle or enriched garnet-bearing pyroxenite veins.
3. The data are consistent with a melting process in which ^{238}U and ^{226}Ra excesses are generated at shallow depths (<60 km) in the melt column, which we interpret to be shallow melting of spinel lherzolite.
4. The equilibrium percolation model seems to be the most appropriate model to choose based on the excesses of shorter-lived nuclides in the U-series decay chain (^{226}Ra and ^{231}Pa). However, it is important to note that this particular data set does not preclude dynamic melting as formalized by McKenzie [68].
5. Equilibrium percolation modeling provides permissible evidence that ^{238}U, ^{231}Pa and ^{226}Ra excesses can be generated in the spinel lherzolite stability field, mainly controlled by diopsidic clinopyroxene, in which $D_{Pa}<D_{Ra}<D_U<D_{Th}$. Targeted disequilibria can mostly be attained at relatively low porosities (~0.1–0.2%), at reasonable upwelling rates (1–2 cm/year) and at a range of column lengths (20–85 km).

Acknowledgements

We thank B. Bourdon and H. Zou for thoughtful and critical reviews. We thank L. Ball (ICP-MS, PIMMS analyst, WHOI), G. Layne (SIMS analyst, WHOI) and P. Janney (PIMMS analyst, Chicago Natural History Museum). This manuscript was prepared while FJT was a post-doctoral researcher at the University of Illinois, Urban-Champaign. This work was supported by NSF grant OCE-9910921 to CCL and NSF grants OCE-9730967 and OCE-0137325 to KWWS. The samples from the Garrett Transform were obtained by the submersible Nautile and its support ship N.O. *Nadir* during a cruise funded and organized by IFREMER. ***[BW]***

Appendix A. Procedures

Concentrations were measured on a Finnigan Mat ELEMENT inductively coupled plasma, magnetic-sector, single-collector mass spectrometer at WHOI. U, Ra and Pa isotopes and some U and Th concentrations were measured via TIMS at UIUC on a VG 354 single-collector mass spectrometer equipped with an ion-counting Daly detector.

A majority of the samples were analyzed for Th isotopes via SIMS on the VG ims 1270 at WHOI

following the procedures of Layne and Sims [50]. Others were analyzed on a ThermoFinnigan Neptune (PIMMS). Th isotopic analyses are made statically, measuring ^{232}Th on a Faraday cup and ^{230}Th on the RPQ channel using the SEM. Using the RPQ on the ThermoFinnigan Neptune, the abundance sensitivity at 95% transmission is ~ 25 ppb over 2 amu, resulting in a tail correction of ^{232}Th on ^{230}Th of 0.7% for ratios of 3×10^5 and 0.3% for ratios of 1.5×10^5. To correct for both instrumental mass fractionation between masses 230 and 232 and the relative difference in the efficiency of the Faraday and SEM detectors, Th isotopic measurements are corrected based upon a linear interpolation of the ^{238}U/^{236}U measured in the NBS U010 standard interspersed between each sample, and normalized to its certified value (14,535 ± 149). Reproducibility in the measured ^{238}U/^{236}U of the NBS U010 ($n=91$) is 0.6% (2σ). Replicate measurements of ^{232}Th/^{230}Th in synthetic and rock Th isotopic standards provide an overall reproducibility on the ^{232}Th/^{230}Th of 0.1–0.5% (2σ) and show excellent agreement with their ''known'' values established by other techniques, supporting the reliability and accuracy of this method [51].

Sr isotopes were measured on the Micromass Isoprobe (PIMMS) fitted with a WARP filter at the Field Museum of Natural History, Chicago, Illinois. All isotopic measurements were made using static measurements on Faraday cups. Samples were run in ~ 5% HNO_3 and diluted so as to create ~ $2–8 \times 10^{-11}$ A beam on ^{88}Sr (~ 250 ppb). NBS 987 (200 ppb), which yields ~ $4–5 \times 10^{-11}$ A on ^{88}Sr, was analyzed before running samples, midway through the day, and at the end of the day to ensure continuity. Backgrounds were measured on the ^{88}Sr peak position and are less than 1×10^{-14} A. Samples were introduced via a CETAC Aridus desolvating nebulizer. Repeat measurements on NBS 987 gave ^{87}Sr/^{86}Sr = 0.710333 ± 7 ($n=3$). Using the offset of NBS 987 from its accepted value of ^{87}Sr/^{86}Sr = 0.710255, a correction (0.000078) was applied to each sample.

In the case of measuring Sr isotopes, the mass interferences that were monitored were Kr and Rb. The contribution from ^{86}Kr on ^{86}Sr (from trace impurities in Ar carrier gas) was less than 5×10^{-15} A and was corrected by measuring an on-peak blank for 60 s prior to every analysis and by monitoring the ^{82}Kr/^{86}Sr ratio during the run. The interference of ^{87}Rb on the ^{87}Sr peak is minimized as much as possible through careful chromatographic separations. However, complete removal of Rb from the sample is not always possible. The contribution of ^{87}Rb to the ^{87}Sr/^{86}Sr ratio is determined from the ^{85}Rb/^{86}Sr ratio, which is multiplied by the natural ^{87}Rb/^{85}Rb and subtracted from the measured ^{87}Sr/^{86}Sr ratio. In all samples, the Rb correction was very small (≤ 0.00002 correction to ^{87}Sr/^{86}Sr or ~ 0.03%).

References

[1] C.H. Langmuir, E.M. Klein, T. Plank, Petrological systematics of mid-ocean ridge basalts: constraints on melt generation beneath ocean ridges, in: J.P. Morgan, D.K. Blackman, J.M. Sinton (Eds.), Mantle Flow and Melt Generation at Mid-Ocean Ridges, Geophys. Monogr. Ser., vol. 71, 1992, pp. 183–280.

[2] C.C. Lundstrom, J. Gill, Q. Williams, M.R. Perfit, Mantle melting and basalt extraction by equilibrium porous flow, Science 270 (1995) 1958–1961.

[3] B. Bourdon, A. Zindler, T. Elliott, C.H. Langmuir, Constraints on mantle melting at mid-ocean ridges from global (super 238) U-(super 230) Th disequilibrium data, Nature (London) 384 (1996) 231–235.

[4] Y. Niu, R. Batiza, Trace element evidence from seamounts for recycled oceanic crust in the Eastern Pacific mantle, Earth Planet. Sci. Lett. 148 (1997) 471–483.

[5] J.I. Wendt, Y. Niu, M. Batiza, M. Regelous, K.D. Collerson, Extreme mantle source heterogeneities beneath the northern East Pacific Rise (EPR): trace element and Nd–Pb–Sr isotope evidence from near-ridge seamounts, EUG IX, Terra Nova Abstr., (Suppl. 9) (1997) 60.

[6] J.I. Wendt, M. Regelous, R. Hékinian, Y. Niu, K.D. Collerson, The nature of mantle heterogeneities and melt extraction processes beneath the East Pacific Rise (EPR); evidence from ultra-depleted lavas in the Garrett Transform, Eos 78 (1997) F675.

[7] D.J. Fornari, M.R. Perfit, J.F. Allan, R. Batiza, R. Haymon, A. Barone, W.B.F. Ryan, T. Smith, T. Simkin, M.A. Luckman, Geochemical and structural studies of the Lamont Seamounts: seamounts as indicators of mantle processes, Earth Planet. Sci. Lett. 89 (1988) 63–83.

[8] D.J. Fornari, M.R. Perfit, J.F. Allan, R. Batiza, Small-scale heterogeneities in depleted mantle sources: near-ridge seamount lava geochemistry and implications for mid-ocean ridge magmatic processes, Nature 331 (1988) 511–513.

[9] J.F. Allan, R. Batiza, M.R. Perfit, D.J. Fornari, R.O. Sack, Petrology of lavas from the Lamont Seamount chain and adjacent East Pacific Rise, 10°N, J. Petrol. 30 (1989) 1245–1298.

[10] J.H. Natland, Partial melting of a lithologically heterogeneous mantle: inferences from crystallization histories of magnesian abyssal tholeiites from the Siqueiros Fracture

Zone, in: A.D. Saunders, M.J. Norry (Eds.), Magmatism in the Ocean Basins, Spec. Publ.-Geol. Soc. Lond., vol. 42, 1989, pp. 41–70.
[11] M.R. Perfit, D.J. Fornari, M.C. Smith, J.F. Bender, C.H. Langmuir, R.M. Haymon, Small-scale spatial and temporal variations in mid-ocean ridge crest magmatic processes, Geology 22 (1994) 375–379.
[12] M.R. Perfit, D.J. Fornari, W.I. Ridley, P.D. Kirk, J. Casey, K.A. Kastens, J.R. Reynolds, M. Edwards, D. Desonie, R. Shuster, S. Paradis, Recent volcanism in the Siqueiros transform fault: picritic basalts and implications for MORB magma genesis, Earth Planet. Sci. Lett. 141 (1996) 91–108.
[13] S.J. Goldstein, M.R. Perfit, R. Batiza, D.J. Fornari, M.T. Murrell, Off-axis volcanism at the East Pacific Rise detected by uranium-series dating of basalts, Nature (London) 367 (1994) 157–159.
[14] M. Spiegelman, J.R. Reynolds, Combined dynamic and geochemical evidence for convergent melt flow beneath the East Pacific Rise, Nature 402 (1999) 282–285.
[15] K.W. Sims, S.J. Goldstein, J. Blichert-Toft, M.R. Perfit, P. Kelement, D.J. Fornari, P. Michael, M.T. Murrell, S.R. Hart, D.J. DePaolo, G. Layne, L. Ball, M. Jull, J. Bender, Chemical and isotopic constraints on the generation and transport of magma beneath the East Pacific Rise, Geochim. Cosmochim. Acta 66 (2002) 3481–3504.
[16] C.J. Allegre, D.L. Turcotte, Implications of a two-component marble-cake mantle, Nature 323 (1986) 123–127.
[17] K.W. Sims, D.J. DePaolo, M.T. Murrell, W.S. Baldridge, S.J. Goldstein, D.A. Clague, Mechanisms of magma generation beneath Hawaii and mid-ocean ridges: U/Th and Sm/Nd isotopic evidence, Science 267 (1995) 508–512.
[18] D. Bideau, R. Hekinian, A dynamic model for generating small-scale heterogeneities, J. Geophys. Res. 100 (1995) 10141–10162.
[19] Y. Niu, M. Regelous, I. Wendt, R. Batiza, M. O'Hara, Geochemistry of near-EPR seamounts: importance of source versus process and the origin of enriched mantle component, Earth Planet. Sci. Lett. 199 (2002) 327–345.
[20] C.C. Lundstrom, D.E. Sampson, M.R. Perfit, J. Gill, Q. Williams, Insights into mid-ocean ridge basalt petrogenesis; U-series disequilibria from the Siqueiros Transform, Lamont Seamounts, and East Pacific Rise, J. Geophys. Res., B Solid Earth Planets 104 (1999) 13035–13048.
[21] P.J. Le Roux, A.P. le Roex, J.G. Schilling, N. Shimizu, W.W. Perkins, N.J.G. Pearce, Mantle heterogeneity beneath the southern Mid-Atlantic Ridge; trace element evidence for contamination of ambient asthenospheric mantle, Earth Planet. Sci. Lett. 203 (2002) 479–498.
[22] M. Jull, P.B. Kelemen, K. Sims, Consequences of diffuse and channelled porous melt migration on uranium series disequilibria, Geochim. Cosmochim. Acta 66 (2002) 4133–4148.
[23] M. Spiegelman, P. Kelemen, Extreme chemical variability as a consequence of channelized melt transport, Geochem. Geophys. Geosyst. 4 (2003) DOI: 10.1029/2002GC000336.
[24] M. Spiegelman, P.B. Kelemen, E. Aharonov, Causes and consequences of flow organization during melt transport; the reaction infiltration instability in compactible media, J. Geophys. Res. 106 (2001) 2061–2077.
[25] K.H. Rubin, J.D. Macdougall, (super 226) Ra excesses in mid-ocean-ridge basalts and mantle melting, Nature (London) 335 (1988) 158–161.
[26] K.H. Rubin, J.D. Macdougall, Dating of neovolcanic MORB using (226Ra/230Th) disequilibrium, Earth Planet. Sci. Lett. 101 (1990) 313–322.
[27] S.J. Goldstein, M.T. Murrell, D.R. Janecky, Th and U isotopic systematics of basalts from the Juan de Fuca and Gorda ridges by mass spectrometry, Earth Planet. Sci. Lett. 96 (1989) 134–146.
[28] S.J. Goldstein, M.T. Murrell, D.R. Janecky, J.R. Delaney, D.A. Clague, Geochronology and petrogenesis of MORB from the Juan de Fuca and Gorda Ridges by 238U–230Th disequilibrium, Earth Planet. Sci. Lett. 107 (1992) 25–41.
[29] S.J. Goldstein, M.T. Murrell, R.W. Williams, (super 231) Pa and (super 230) Th chronology of mid-ocean ridge basalts, Earth Planet. Sci. Lett. 115 (1993) 151–159.
[30] A.M. Volpe, S.J. Goldstein, (super 226) Ra–(super 230) Th disequilibrium in axial and off-axis mid-ocean ridge basalts, Geochim. Cosmochim. Acta 57 (1993) 1233–1241.
[31] K.H. Rubin, J.D. Macdougall, M.R. Perfit, (super 210) Po–(super 210) Pb dating of Recent volcanic eruptions on the sea floor, Nature (London) 368 (1994) 841–844.
[32] C.C. Lundstrom, J. Gill, Q. Williams, B.B. Hanan, Investigating solid mantle upwelling beneath mid-ocean ridges using U-series disequilibria: II. A local study at 33 degrees S Mid-Atlantic Ridge, Earth Planet. Sci. Lett. 157 (1998) 167–181.
[33] C.C. Lundstrom, Q. Williams, J.B. Gill, Investigating solid mantle upwelling rates beneath mid-ocean ridges using U-series disequilibria: 1. A global approach, Earth Planet. Sci. Lett. 157 (1998) 151–165.
[34] K.W.W. Sims, D.J. DePaolo, M.T. Murrell, W.S. Baldridge, S.J. Goldstein, D.A. Clague, M. Jull, Porosity of the melting zone and variations in the solid upwelling rate beneath Hawaii: inferences from 238U–230Th–226Ra and 235U–231Pa disequilibria, Geochim. Cosmochim. Acta 63 (1999) 4119–4138.
[35] K.W.W. Sims, J. Blichert-Toft, D. Fornari, M.R. Perfit, S. Goldstein, P. Johnson, D.J. DePaolo, S.R. Hart, M.T. Murrell, P. Michaels, G. Layne, L. Ball, Aberrant youth: chemical and isotopic constraints on the young off-axis lavas of the East Pacific Rise, Geochem. Geophys. Geosyst. 4 (2003) DOI: 10.1029/2002GC000443.
[36] B. Bourdon, C.H. Langmuir, A. Zindler, Ridge–hotspot interaction along the Mid-Atlantic Ridge between 37 degrees 30′ and 40 degrees 30′N; the U–Th disequilibrium evidence, Earth Planet. Sci. Lett. 142 (1996) 175–189.
[37] T. Elliott, Fractionation of U and Th during mantle melting: a reprise, Chem. Geol. 139 (1997) 165–183.
[38] B. Bourdon, K.W.W. Sims, U-series constraints on intraplate basaltic magmatism, in: B. Bourdon, G.M. Henderson, C.C. Turner, S.P. Turner (Eds.), Uranium-Series Geochemistry, Reviews in Mineralogy and Geochemistry, vol. 52, Geochemical Society, Mineralogical Society of America, 2003, pp. 215–254.

[39] C.C. Lundstrom, Uranium-series disequilibria in mid-ocean ridege basalts: observations and models of basalt genesis, in: B. Bourdon, G.M. Henderson, C.C. Lundstrom, S.P. Turner (Eds.), Uranium-Series Geochemistry, Reviews in Mineralogy and Geochemistry, vol. 52, Geochemical Society, Mineralogical Society of America, 2003, pp. 175–214.
[40] M. Condomines, O. Sigmarsson, 238U–230Th disequilibria and mantle melting processes: a discussion, Chem. Geol. 162 (2000) 95–104.
[41] P.J. Fox, J.A. Gallo, Transforms of the eastern central Pacific, in: N.E.L. Winterer, D.M. Hussomg, R.D. Decker (Eds.), The Geology of North America, Geol. Soc. Am., (1989) 111–123.
[42] R. Hékinian, D. Bideau, M. Cannat, J. Francheteau, R. Hébert, Volcanic activity and crust–mantle exposure in the ultrafast Garrett Transform fault near 13°28′S in the pacific, Earth Planet. Sci. Lett. 108 (1992) 259–275.
[43] R. Hékinian, D. Bideau, R. Hébert, Y. Niu, Magmatism in the Garrett Transform fault (East Pacific Rise near 13°27′S), J. Geophys. Res. 100 (1995) 10163–10185.
[44] J.I. Wendt, M. Regelous, Y. Niu, R. Hékinian, K.D. Collerson, Geochemistry of lavas from the Garrett Transform Fault: insights into mantle heterogeneity beneath the eastern Pacific, Earth Planet. Sci. Lett. 173 (1999) 271–284.
[45] R. Hébert, R. Hékinian, D. Bideau, Primitive intratransform volcanism at Garrett Transform Fault (East Pacific Rise), Can. J. Earth Sci. 34 (1997) 1101–1117.
[46] J.M. Sinton, S.M. Smaglik, J.J. Mahoney, K. Macdonald, Magmatic processes at superfast spreading mid-ocean ridges: glass compositional variations along the East Pacific Rise 13°23′S, J. Geophys. Res. 96 (1991) 6133–6155.
[47] Y. Niu, R. Hékinian, Basaltic liquids and harzburgitic residues in the Garrett Transform: a case study at fast-spreading ridges, Earth Planet. Sci. Lett. 146 (1997) 243–258.
[48] A.H. Andrews, K.H. Coale, J.L. Nowicki, C.C. Lundstrom, Z. Palacz, E.J. Burton, G.M. Caillet, Applications of an ion-exchange separation technique and thermal ionization mass spectrometry to 226Ra determination in otoliths for radiometric are determination of long-lived fishes, Can. J. Fish. Aquat. Sci. 56 (1999) 1329–1338.
[49] D.A. Pickett, M.T. Murrell, R.W. Williams, Determination of femtogram quantities of protactinium in geologic samples by thermal ionization mass spectrometry, Anal. Chem. 66 (1994) 1044–1049.
[50] G.D. Layne, K.W. Sims, Secondary ion mass spectrometry for the measurement of 232Th/230Th in volcanic rocks, Int. J. Mass Spectrom. 203 (2000) 187–198.
[51] L. Ball, K.W.W. Sims, S. Weyer, J. Schwieters, Measurement of 232Th/230Th in volcanic rocks by PIMMS using ThermoFinnigan Neptune, Abstracts of the 12th annual V.M. Goldschmidt Conference, Geochim. Cosmochim. Acta 66 (2002) 47.
[52] D. Thurber, Anomalous 234U/238U in nature, J. Geophys. Res. 67 (1967) 4518.
[53] T.-L. Ku, K.G. Knauss, G.G. Mathieu, Uranium in open ocean: concentration and isotopic composition, Deep-Sea Res. 24 (1977) 1005–1017.
[54] I. Reinitz, K.K. Turekian, 230Th/238U and 226Ra/230Th fractionation in young basaltic glasses from the East Pacific Rise, Earth Planet. Sci. Lett. 94 (1989) 99–207.
[55] D. Ben Othman, C.J. Allegre, U–Th isotopic systematics at 13°N east Pacific Ridge segment, Earth Planet. Sci. Lett. 98 (1990) 129–137.
[56] P. Beattie, Uranium–thorium disequilibria and partitioning on melting of garnet peridotite, Nature (London) 363 (1993) 63–65.
[57] T.Z. LaTourrette, A.K. Kennedy, G.J. Wasserburg, Thorium–uranium fractionation by garnet; evidence for a deep source and rapid rise of oceanic basalts, Science 261 (1993) 739–742.
[58] E.H. Hauri, T.P. Wagner, T.L. Grove, Experimental and natural partitioning of Th, U, Pb and other trace elements between garnet, clinopyroxene and basaltic melts, in: S.F. Foley, S.R. van der Laan (Eds.), Trace-Element Partitioning with Application to Magmatic Processes, Chem. Geol., vol. 117, Elsevier, Amsterdam, Netherlands, 1994, pp. 149–166.
[59] V.J.M. Salters, J. Longhi, Trace element partitioning during the initial stages of melting beneath mid-ocean ridges, Earth Planet. Sci. Lett. 166 (1999) 15–30.
[60] B.J. Wood, J.D. Blundy, J.A.C. Robinson, The role of clinopyroxene in generating U-series disequilibrium during mantle melting, Geochim. Cosmochim. Acta 63 (1999) 1613–1620.
[61] D. Landwehr, J. Blundy, P.E.M. Chamorro, E. Hill, B. Wood, U-series disequilibria generated by partial melting of spinel lherzolite, Earth Planet. Sci. Lett. 188 (2001) 329–348.
[62] M.M. Hirschmann, E.M. Stolper, A possible role for garnet pyroxenite in the origin of the "garnet signature" in MORB, Contrib. Mineral. Petrol. 124 (1996) 185–208.
[63] M. Condomines, 230Th–238U radioactive disequilibria in tholeiites from the FAMOUS zone (Mid-Atlantic Ridge, 36°50′N); Th and Sr isotopic geochemistry, Earth Planet. Sci. Lett. 55 (1981) 247–256.
[64] K.W. Sims, N. Mattielli, T. Elliott, P. Kelemen, D.J. DePaolo, D.F. Mertz, C. Devey, M.T. Murrell, 238U and 230Th excesses in Kolbeinsey ridge basalts, Eos Trans. AGU 82 (47) (Fall Meeting Supplement, Abstract V12A-0952).
[65] H. Zou, A. Zindler, Y. Niu, Constraints on melt movement beneath the East Pacific Rise from 230Th–238U disequilibrium, Science 295 (2002) 107–110.
[66] T.Z. LaTourrette, D.S. Burnett, Experimental determination of U and Th partitioning between clinopyroxene and natural and synthetic basaltic liquid, Earth Planet. Sci. Lett. 110 (1992) 227–244.
[67] C.C. Lundstrom, H.F. Shaw, F.J. Ryerson, D.L. Phinney, J.B. Gill, Q. Williams, Compositional controls on the partitioning of U, Th, Ba, Pb, Sr and Zr between clinopyroxene and haplobasaltic melts; implications for uranium series disequilibria in basalts, Earth Planet. Sci. Lett. 128 (1994) 407–423.
[68] D. McKenzie, The extraction of magma form the crust and mantle, Earth Planet. Sci. Lett. 74 (1985) 81–91.
[69] R.W. Williams, J.B. Gill, Effects of partial melting on the uranium decay series, Geochim. Cosmochim. Acta 53 (1989) 1607–1619.

[70] R.J. Kinzler, T.L. Grove, Primary magmas of mid-ocean ridge basalts: 2. Applications, J. Geophys. Res. 97 (1992) 6907–6926.
[71] E. Klein, C.H. Langmuir, Global correlations of ocean ridge basalt chemistry with axial depth and crustal thickness, J. Geophys. Res. 92 (1987) 8089–8115.
[72] P.D. Kirk, M.R. Perfit, W.I. Ridley, D.J. Fornari, J.F. Casey, Sources and processes involved in the petrogenesis of Siqueiros transform basalts, Eos Trans.-Am. Geophys. Union 75 (1994) 745.
[73] K.S. Harpp, W.M. White, The East Pacific Rise magma chamber (9 degrees–10 degrees N); isotopic and trace element constraints, Eos Trans.-Am. Geophys. Union 76 (1995) 694.
[74] C.C. Lundstrom, J. Gill, Q. Williams, A geochemically consistent hypothesis for MORB generation, in: N. Rogers (Ed.), Rates and Timescales of Magmatic Processes, Elsevier, Amsterdam, Netherlands, 2000.
[75] C.C. Lundstrom, An experimental investigation of the diffusive infiltration of alkalis into partially molten peridotite: implications for mantle melting process, Geochem. Geophys. Geosyst. (2003) (DOI10.1029/2001GC000224).
[76] D. McKenzie, The generation and compaction of partially molten rock, J. Petrol. 25 (1984) 713–765.
[77] M. Spiegelman, T. Elliott, Consequences of melt transport for uranium series disequilibrium in young lavas, Earth Planet. Sci. Lett. 118 (1993) 1–20.
[78] P.D. Asimow, M.M. Hirschmann, M.S. Ghiorso, M.J. O'Hara, E.M. Stolper, The effect of pressure-induced solid–solid phase transitions on decompression melting of the mantle, Geochim. Cosmochim. Acta 59 (1995) 4489–4506.
[79] C. Richardson, D. McKenzie, Radioactive disequilibria from 2D models of melt generation by plumes and ridges, Earth Planet. Sci. Lett. 128 (1994) 425–437.
[80] M. Spiegelman, UserCalc: a web-based uranium series calculator for magma-migration problems, Geochem. Geophys. Geosyst. 1 (2000) (1999GC000030).
[81] J.M. Brenan, H.F. Shaw, F.J. Ryerson, D.L. Phinney, Mineral–aqueous fluid partitioning of trace elements at 900 °C and 2.0 Gpa: constraints on the trace element chemistry of mantle and deep crustal fluids, Geochim. Cosmochim. Acta 59 (1995) 3331–3350.
[82] H. Keppler, Constraints from partitioning experiments on the composition of subduction-zone fluids, Nature 380 (1996) 237–240.
[83] O. Sigmarsson, M. Condomines, J.D. Morris, R.S. Harmon, Uranium and 10Be enrichments by fluids in Andean arc magmas, Nature 346 (1990) 163–165.
[84] J.B. Gill, J.D. Morris, R.W. Johnson, Timescale for producing the geochemical signature of island arc magmas: U–Th–Po and Be–B systematics in recent Papua New Guinea lavas, Geochim. Cosmochim. Acta 57 (1993) 1427–1442.
[85] F. McDermott, M.J. Defant, C.J. Hawkesworth, R.C. Maury, J.L. Joron, Isotope and trace element evidence for three component mixing in the genesis of the North Luzon arc lavas (Philippines), Contrib. Mineral. Petrol. 113 (1993) 9–23.
[86] M.K. Reagan, J.D. Morris, E.A. Herrstrom, M.T. Murrell, Uranium series and beryllium isotope evidence for an extended history of subduction modification of the mantle below Nicaragua, Geochim. Cosmochim. Acta 58 (1994) 4199–4212.
[87] T. Elliott, T. Plank, A. Zindler, W. White, B. Bourdon, Element transport from slab to volcanic front at the Mariana arc, J. Geophys. Res. 102 (1997) 14991–15019.
[88] S. Turner, C. Hawkesworth, Constraints on flux rates and mantle dynamics beneath island arcs from Tonga–Kermadec, Nature 389 (1997) 568–573.
[89] S. Turner, C. Hawkesworth, N. Rogers, J. Bartlett, T. Worthington, J. Hergt, J. Pearce, I. Smith, 238U–230Th disequilibria, magma petrogenesis and flux rates beneath the depleted Tonga–Kermadec island arc, Geochim. Cosmochim. Acta 61 (1997) 4855–4884.
[90] S. Turner, F. McDermott, C. Hawkesworth, P. Kepzhinskas, U-series study of Kamchatka; constraints on source composition and melting conditions, Contrib. Mineral. Petrol. 133 (1998) 217–234.
[91] S. Turner, D.W. Peate, C. Hawkesworth, S.M. Eggins, A.J. Crawford, Two mantle domains and the times scales of fluid transfer beneath the Vanuatu arc, Geology 27 (1999) 963–966.
[92] S. Turner, R.M.M. George, P.J. Evans, C.J. Hawkesworth, G.F. Zellmer, Time-scales of magma formation, ascent and storage beneath subduction-zone volcanoes, Philos. Trans. R. Soc. Lond., A 238 (2000) 1443–1464.
[93] R.M. George, S.P. Turner, C.J. Hawkesworth, C. Nye, Along-arc U–Th–Ra systematics in the Aleutians, Eos 82 (1999) 1023.
[94] G. Zellmer, S. Turner, C. Hawkesworth, Timescales of destructive plate margin magmatism: new insights from Santorini, Aegean volcanic arc, Earth Planet. Sci. Lett. 174 (2000) 265–281.
[95] J.D. Macdougall, G. Lugmair, Sr and Nd isotopes in basalts from the East Pacific Rise; significance for mantle heterogeneity, Earth Planet. Sci. Lett. 77 (1986) 273–284.
[96] S. Newman, R.C. Finkel, J.D. MacDougall, (super 230) Th–(super 238) U disequilibrium systematics in oceanic tholeiites from 21 degrees N on the East Pacific Rise, Earth Planet. Sci. Lett. 65 (1983) 17–33.
[97] A.S. Davis, D. Clague, Geochemistry, mineralogy, and petrogenesis of basalt from the Gorda Ridge, J. Geophys. Res. 92 (1987) 10467–10483.
[98] J.S. Eaby, D.A. Clague, J.R. Delaney, Sr isotopic variations along the Juan de Fuca Ridge, J. Geophys. Res. 89 (1984) 7883–7890.
[99] B. Dupre, D. Lambret, D. Rousseau, C.J. Allegre, Limitations on the scale of mantle heterogeneities under oceanic ridges, Nature 294 (1981) 552–554.
[100] C. Hemond, M. Condomines, S. Fourcade, C.J. Allegre, N. Oskarsson, M. Javoy, Thorium, strontium and oxygen isotopic geochemistry in Recent tholeiites from Iceland; crustal influence on mantle-derived magmas, Earth Planet. Sci. Lett. 87 (1988) 273–285.
[101] O. Sigmarsson, M. Condomines, S. Fourcade, A detailed

Th, Sr and O isotope study of Hekla; differentiation processes in an Icelandic volcano, Contrib. Mineral. Petrol. 112 (1992) 20–34.
[102] O. Sigmarsson, M. Condomines, S. Fourcade, Mantle and crustal contribution in the genesis of recent basalts from off-rift zones in Iceland; constraints from Th, Sr and O isotopes, Earth Planet. Sci. Lett. 110 (1992) 149–162.
[103] S. Newman, R. Finkel, J. Macdougall, Comparison of 230Th–238U disequilibrium systematics in lavas from three hot spot regions; Hawaii, Prince Edward and Samoa, Geochim. Cosmochim. Acta 48 (1984) 315–324.
[104] R.W. Williams, J.B. Gill, Th isotope and U-series disequilibria in some alkali basalts, Geophys. Res. Lett. 19 (1992) 139–142.
[105] E. Widom, R.W. Carlson, J.B. Gill, H.U. Schmincke, Th–Sr–Nd–Pb isotope and trace element evidence for the origin of the Sao Miguel enriched mantle source, Chem. Geol. 140 (1997) 49–68.
[106] D.R. Hilton, J. Barling, G.E. Wheiler, The effect of shallow-level contamination on the helium isotope systematics of ocean island lavas, Nature 348 (1990) 59–62.
[107] C. Claude-Ivanaj, J.-L. Joron, C. Allegre, 238U–230Th–226Ra fractionation in historical lavas from the Azores: long-lived source heterogeneity versus metasomatism fingerprints, Chem. Geol. 176 (2001) 295–310.
[108] L. Dosso, H. Bougault, C. Langmuir, C. Bollinger, O. Bonnier, J. Etoubleau, The age and distribution of mantle heterogeneity along the Mid-Atlantic Ridge (31–41°N), Earth Planet. Sci. Lett. 170 (1999) 269–286.
[109] L.J. Le Roux, L.E. Glendenin, Half-life of 232Th, Proceedings of the National Meeting on Nuclear Energy, 1963, pp. 83–94 (Abstract).
[110] H. Cheng, R.L. Edwards, J. Hoff, C.D. Gallup, D.A. Richards, Y. Asmerom, The half-lives of uranium-234 and thorium-230, Chem. Geol. 169 (2000) 17–33.
[111] J. Robert, C.F. Miranda, R. Muxart, Mesure de la période du protactinium-231 par microcalorimétrie, Radiochim. Acta 11 (1963) 104–108.